

Electronic excitations and the tunneling spectra of metallic nanograins

Gustavo A. Narvaez^{a,b} and George Kirczenow^b

^a *Department of Physics, The Ohio State University, Columbus, Ohio 43210*

^b *Department of Physics, Simon Fraser University, Burnaby, British Columbia, Canada V5A 1S6*

(Dated: November 14, 2018)

Tunneling-induced electronic excitations in a metallic nanograin are classified in terms of *generations*: subspaces of excitations containing a specific number of electron-hole pairs. This yields a hierarchy of populated excited states of the nanograin that strongly depends on (a) the available electronic energy levels; and (b) the ratio between the electronic relaxation rate within the nanograin and the bottleneck rate for tunneling transitions. To study the response of the electronic energy level structure of the nanograin to the excitations, and its signature in the tunneling spectrum, we propose a microscopic mean-field theory. Two main features emerge when considering an Al nanograin coated with Al oxide: (i) The electronic energy response fluctuates strongly in the presence of disorder, from level to level and excitation to excitation. Such fluctuations produce a dramatic sample dependence of the tunneling spectra. On the other hand, for excitations that are energetically accessible at low applied bias voltages, the magnitude of the response, reflected in the renormalization of the single-electron energy levels, is smaller than the average spacing between energy levels. (ii) If the tunneling and electronic relaxation time scales are such as to admit a significant non-equilibrium population of the excited nanoparticle states, it should be possible to realize much higher spectral densities of resonances than have been observed to date in such devices. These resonances arise from tunneling into ground-state and excited electronic energy levels, as well as from charge fluctuations present during tunneling.

PACS numbers: 73.22.-f, 73.22.Dj

I. INTRODUCTION

In the late '90s it was demonstrated that single quantum level tunneling spectroscopy is a powerful tool for studying the physics of simple, noble, and magnetic nanoscale metals. Ralph, Black and Tinkham first used this technique to study the electronic energy level structure of *individual* oxide-coated aluminum nanoparticles¹, and it was soon applied to Co, Au, Ag, and Cu nanograins as well^{2,3,4}. Even after several theoretical studies^{5,6,7,8,9}, a key aspect of the data (the unexpectedly high density of resonances in the tunneling spectra of the metal nanograins) remains not fully understood, as was discussed in Ref. 2. More intriguingly, these resonances appear in clusters. As the nanograins are expected to present strong surface disorder, this bunching of resonances seemed to collide with the predictions of random matrix theory for the single-particle energy levels of small disordered conductors¹⁰. In order to explain these experimental features, Agam and co-workers⁵ argued that the electron tunneling may occur under conditions far from equilibrium which would result in the presence of a large number of resonances and bunching. They offered a phenomenological model able to account for some of the observed features. More recently, however, Davidović and Tinkham presented alternate scenarios—charge trapping, single occupancy of Kramers doublets, and non-equilibrium effects—that might be responsible for the bunching of the tunneling resonances that they observed in Au nanoparticles². Furthermore, the present authors developed a microscopic model for the tunneling spectroscopy of these nanoparticles and argued that clustering of resonances should arise naturally in metal

nanograins⁷, even in the absence of the non-equilibrium transport effects introduced by Agam *et al.*⁵ It has also been shown recently that charge-fluctuations that are present during the electron tunneling should generate *additional* tunneling resonances,⁸ not considered in previous theories, and that penetration of environmental electric fields into metal nanoparticles can have striking effects on their tunneling spectra.⁹

In this paper, we classify the electronic excitations that may take place during electron tunneling within an ultra-small metallic grain in terms of *generations*: subspaces of excitations with a specific number of electron-hole pairs. Furthermore, we propose a general microscopic mean-field model to calculate the quasi-particle energy levels in the presence of an excitation; such a model has not been previously presented in the literature, to the best of our knowledge. The generations form a hierarchy that strongly depends on (i) the number of available electronic energy levels for tunneling, and (ii) the ratio between the electronic relaxation rate within the nanograin and the bottleneck rate for tunneling transitions. The latter is quite sensitive to the thickness of the tunneling barriers. The applied bias voltage, and characteristics of the device—grain-lead capacitances, charging energy, and typical energy spacing between electronic energy levels in the nanograin—determine the number of electronic configurations that are present in a generation. Finally, we present detailed results of the response of the electronic energy structure to the excitations in an ultra-small aluminum grain coated with Al oxide. We find that: (i) The renormalization of the electronic energy levels in the ground states fluctuates strongly from level to level, and excitation to excitation due to the stochasticity of the

confined electronic wavefunctions that is imposed by the disorder present in the grain; these fluctuations depend dramatically on the specific realization of the disorder. (ii) The average single-electron energy level spacing in the excited states remains nearly unchanged when compared with the value obtained in the ground-state; changes are within a few percent. (iii) If the kinetics of the tunneling transitions, and intragrain electronic relaxation, are such as to admit a significant population of excited states, then the predicted number of tunneling resonances can be *much* higher than has been observed to date in tunneling experiments in non-magnetic nanoparticles. (iv) Disorder is responsible for a strong sample-dependence of (a) the number of resonances present, as clusters, in the tunneling spectrum, and (b) the spectral width of such clusters as a function of the applied bias voltage.

II. MECHANISM FOR ELECTRONIC EXCITATIONS AND THEIR SIGNATURE IN NONEQUILIBRIUM TUNNELING SPECTROSCOPY

We are interested in the electron tunneling regime where: (i) the Coulomb charging energy¹¹ (U) of the grain that results from adding or removing a valence electron, is greater than the expected average particle-in-a-box level spacing (δ) around the Fermi energy. This is often the experimental situation^{1,2,3,4}. (ii) The electronic relaxation rate (Γ_r) within the grain is much *smaller* than the bottleneck tunneling rate (Γ), and (iii) tunneling leaves the grain with a surplus or deficit of one electron with respect to the n_0 valence electrons that make the grain neutral. In this regime, after an electron tunnels in *and* out, the grain may be left in an excited electronic state while still being neutral. Therefore, charge transport may take place via excited (non-equilibrium) nanoparticle states. This mechanism for generating electronic excitations, that may be reflected in the energy spectra of metallic nanograins, was first exploited by Agam, Wingreen, Altshuler, Ralph and Tinkham⁵ (AWARTi) to explain tunneling spectroscopy experiments in Al nanoparticles. However, the original AWARTi model was spinless and, more importantly, the effects of the electronic excitations on the electronic energy levels were treated only within the framework of random matrix theory.

Let us now discuss the *genesis* of the tunneling-induced electronic excitations. We begin by considering a two-terminal device consisting of macroscopic source (S) and drain (D) electrodes separated by a thin insulating layer from a metallic nanoparticle (d). Following the Orthodox theory of Coulomb blockade,¹¹ the electrochemical potential of the source (drain) electrode is set to: $\mu^{S(D)}(V) = E_F + (-)(C_{D(S)}/C_\Sigma)eV$; where V is the applied bias voltage, e the magnitude of the electron charge, and $C_\Sigma = C_S + C_D$ with $C_{S(D)}$ the capacitance between electrode $S(D)$ and the nanoparticle. The quantum na-

ture of the nanoparticle is taken into account through its discrete electronic structure. For definiteness, we shall assume the nanoparticle to have spin-degenerate single-electron energy levels $|\psi_a\rangle$ with energy E_a , and a fully (doubly) occupied Fermi level ($|\psi_F\rangle$) at energy E_F [see Fig. 1(a)].¹² Furthermore, by adopting $C_D/C_S > 1$ the onset of tunneling corresponds to the injection of an electron from S into $|\psi_{F+1}\rangle$, with a threshold bias voltage given by $V_{S\rightarrow d}^{th} = (1/e)(C_\Sigma/C_D)(U + E_{F+1} - E_F)$. As the number of electrons inside the grain increases by one, the single-electron energy levels of the grain are renormalized upwards by U , within the constant interaction approximation¹³ [see Fig. 1(a)]. Therefore, the subsequent tunneling processes that can take place are: (i) return of the additional electron from level $|\psi_{F+1}\rangle$ to S or its transmission to D ; or (ii) tunneling to D of one of the electrons populating the single-particle levels whose energy satisfies $E_a + U \geq \mu^D(V_{S\rightarrow d}^{th})$. In the latter case, once the electron is ejected from the grain, the remaining electrons are left in an excited state ($|X_1\rangle$) that corresponds to creating one electron-hole (eh) pair on the ground-state electronic configuration ($|G\rangle$) of the nanoparticle; as exemplified in Fig. 1(a). Note that there are *different* possible $1eh$ -pair electronic excitations depending on which electron is ejected out. (We suppose that no shake-up¹⁴ occurs due to the creation of the $1eh$ -pair excitation.) The slow electronic relaxation within the grain, compared with the bottleneck tunneling rate (recall the assumption that $\Gamma/\Gamma_r \gg 1$) makes it possible to generate another family of excitations, namely, $2eh$ -pair excitations [see Fig. 1(b)]. The latter, however, require *two* consecutive tunneling events for their creation. It should be noted that the number of possible $2eh$ -pair states is greater than that of $1eh$ -pair states.

It is important to notice that the multi- eh -pair excitations only arise as a consequence of *multiple* sequential tunneling, as described above. Hence, excited states are likely to exist only if Γ_r is many times *smaller* than Γ . Within this context, it is convenient to introduce the concept of *generations* of excitations: We define a *generation* to be the set of electronic configurations that contain a specific number of eh -pair excitations due to consecutive electron tunneling in and out of the grain. Hence, generation n ($G\#n$) contains the subset of n eh -pair excitations that arise after n such consecutive pairs of tunneling events. Figure 1(b) shows examples of members of generation 1 and generation 2, indicated by $G\#1$ and $G\#2$. It should be clear that the generations constitute a *hierarchy*: It is not possible to have an element of generation- n without having generated previously elements of its $n-1$, $n-2$, $n-3$, \dots , 1 ancestors. Hence, in order for n eh -pair excitations to occur with significant probability the bottleneck tunneling time (Γ^{-1}) should be nearly $2n$ times *smaller* than the electronic relaxation time (Γ_r^{-1}). Finally, the applied bias voltage determines the maximum number of generations that may be present in a device, as it constrains the number of available energy levels: The maximum possible number of eh pairs is $2n$ if n levels are

available in the grain for tunneling; therefore, at most $2n$ generations might exist.

To find the *total* number of excitations present in generation n we note that, *contrary* to the case in closed electronic systems, the tunneling-induced electron-hole pair excitations *may have* a net total spin polarization as large as $S_z = S_z^e + S_z^h$; where $S_z^{e(h)}$ is the largest possible total spin polarization of the excited electrons (holes). This leads to a high multiplicity of the electronic configurations that may be present in generation n , as these configurations result from exhausting all the possible electron and hole arrangements once the restriction $S_z = 0$ is waived. If N (M) orbitals are available to accommodate the excited electrons (holes), the total number of electronic configurations up to generation n is: $\sum_{i=0}^n \binom{2N}{i} \binom{2M}{i}$; where $2n \leq N$ and the factor of 2 accounts for spin polarization.

The above mechanism for generating electronic excitations within a metallic grain in the Coulomb blockade regime, and the subsequent identification of a hierarchy for these excitations constitutes a generalization of the AWARTi model. In order to invoke this mechanism as a possible interpretation of experimental tunneling spectroscopy data, one has to realize that the one-electron levels in the ground-state of the grain are not spectrally rigid.^{5,14} In particular, a net electronic interaction due to the redistribution of the charge within the *neutral* grain due to the excitation renormalizes the one-electron levels: The ground-state single-electron energy level structure ($|\psi_a\rangle, E_a$) changes to ($|\psi_a\rangle_{X_n}^n, E_{aX_n}^n$), with $|X_n\rangle$ an excited state in generation n . Figure 1(c) schematically shows this renormalization in a particular case (see Fig. 2 also). In general, for an excitation with a given number of *eh* pairs, the renormalization of level $|\psi_a\rangle$ depends on the specifics of the excited state, and therefore exhibits *fluctuations*; see Fig. 2. This is due to the stochasticity of the wavefunctions that is imposed by the disorder present in the nanograin.¹⁰ Random matrix theory offers a simple generic approach to modeling this fluctuating renormalization of the one-electron levels. In the presence of single-electron energy level renormalization the tunneling current $I(V)$, at bias voltage V , is determined by a complex master equation that contains the kinetics of all the allowed electron tunneling transitions—including also the renormalized energy levels. Those are given by the following Coulomb blockade threshold equations: $\mu_S(V) \geq E_{aX_n}^n + U$ (for events involving *unoccupied* levels in the grain) and $\mu_D(V) \leq E_{aX_n}^n + U$ (for events involving *occupied* levels in the grain); here $n = 0$ represents the ground-state energy levels ($E_{aX_0}^0 = E_a$). Hence, each time a new tunneling channel is opened a peak in the differential conductance is expected (see below, Sec. IV).

In summary, we have so far introduced the mechanism that creates electronic excitations, recast these excitations as a hierarchy of generations, stated that these excitations renormalize the single-electron energy levels in a complex manner, and discussed the effect of the renor-

malization on the tunneling spectroscopy of the grains. In the following section we present a mean-field theory that can be used to calculate the renormalized one-electron levels of the excited nanoparticle.

III. MEAN-FIELD THEORY OF THE EXCITED QUASI-PARTICLE STATES

A neutral metallic grain with n_0 valence electrons in its ground-state ($|G\rangle$) is the starting point. We then adopt a quasi-particle picture consisting of electronic levels $|\psi_a\rangle$ with energy E_a , and take as $|G\rangle$ the lowest energy n_0 -electrons configuration [see Fig. 1(a)]. By implementing a tight-binding Hamiltonian, E_a and $|\psi_a\rangle$ are calculated taking into account important microscopic features of the nanograin: geometry, structural disorder, and surface chemistry.⁷ In a multi-orbital (s , p , and d) representation, and neglecting spin-orbit coupling, the Hamiltonian is:

$$\mathcal{H} = \sum_{i,\alpha} \varepsilon_i^\alpha c_{i\alpha}^\dagger c_{i\alpha} + \sum_{i,j,\alpha,\alpha'} \mathcal{T}_{j\alpha,i\alpha'} \left(c_{i\alpha'}^\dagger c_{j\alpha} + c_{j\alpha}^\dagger c_{i\alpha'} \right). \quad (1)$$

i (j) labels the lattice site \vec{R}_i (\vec{R}_j) of atom i (j), $c_{i\alpha}^\dagger$ ($c_{i\alpha}$) creates (destroys) an electron on site i , while α (α') indicates the s , p or d orbital. ε_i^α and $\mathcal{T}_{j\alpha,i\alpha'}$ are the Slater-Koster (SK) on-site and hopping parameters.^{15,16}

The metallic nanoparticles that are probed by electron tunneling spectroscopy are passivated with a thin Al-oxide layer and *buried* between two massive electrodes. Hence, to extract data about the morphology of these nanograins is quite difficult. However, their size—several hundreds of atoms—makes it reasonable to model their structure as a crystalline metal *core*, and a disordered superficial (*shell*) region that corresponds to the metal-oxide interface. The disorder present in the surface arises from the chemistry of the oxide layer in combination with surface reconstructions that may occur during growth.¹⁷ The model nanoparticles considered here result from truncating a fcc lattice to a volume \mathcal{V} in a disc or hemisphere geometry.¹⁸ In this case, the coordination numbers of atoms at the surface of the nanoparticle differ from the coordination number of the bulk fcc lattice. This is used to establish a criterion that defines the surface of the particle, and distinguishes between core and shell.⁷ Once the surface atoms are determined we *randomly* choose 50% of those sites to represent O while the other sites correspond to Al. This randomness is the only source of surface disorder we consider.

We adopt as SK parameters in Eq. (1) for the atomic sites in the core of the nanograin those parameterized by Papaconstantopoulos.¹⁹ The aluminum and oxygen sites in the metal-oxide interface (shell), on the other hand, have different SK parameters as a consequence of charge transfer from Al to O. To find the on-site energies for the *charged* oxygen and aluminum atoms in the oxidized shell we combine (i) the Mulliken-Wolfsberg-Helmholz

(MWH) molecular-orbital approach²⁰ with (ii) results of classical molecular dynamics simulations by Campbell and co-workers²¹ that show the metal-oxide interface at the nanometer scale is mainly constituted of intercalated $O^{-1/2}$ and $Al^{+1/2}$. The degree of charge transfer ν determines the on-site energies via the MWH theory: The molecular orbital (μ) energies of atom m are empirically parameterized as $E_\mu^m = E_\mu^m(\nu) = -(A_\mu^m \nu^2 + B_\mu^m \nu + C_\mu^m)$;²⁰ where ν is the excess valence charge: $\nu = (-)1/2$ for Al (O). Hence, the SK on-site energies for the atomic sites *in the oxide layer* are given by $\varepsilon_{Al(O)}^\alpha = -(A_\alpha^{Al(O)}/4 + (-)B_\alpha^{Al(O)}/2 + C_\alpha^{Al(O)} - \Delta)$, with $\Delta = 1.289 Ry$ an off-set energy such that $E_s^{Al}(0) = \varepsilon_{Al}^s$, and the parameters A_α^m , B_α^m , and C_α^m for $m = Al, O$ those of Ref. 20. Finally, we determine the nearest neighbor O - Al hopping SK parameters by assuming an average separation between oxygen and aluminum atoms in the oxide of $d_{Al-O} = 1.8\text{\AA}$,²¹ applying Harrison's model to obtain the two-center transfer integrals²² and then transforming them to find the SK hopping parameters.¹⁹ By taking $d_{O-O} = 3.0\text{\AA}$ ²³ as average separation between O atoms the above procedure leads to the nearest neighbor O - O hopping parameter. We keep the SK hopping parameters for $Al^{+1/2}$ - $Al^{+1/2}$ and $Al^{+1/2}$ - Al the same as those for Al - Al .

Let us now assume that electronic excitations of the n_0 electrons within the grain are present due to the mechanism discussed in Sec II. These excitations can be identified according to the number of electron-hole pairs generated over the ground-state $|G\rangle$. A generic n -electron-hole (n - eh) pair excitation is given by: $|X_n\rangle = |k_1^< k_2^< \dots k_n^<; k_1^> k_2^> \dots k_n^>\rangle = (\prod_{i=1}^n c_{k_i^>}^\dagger)(\prod_{m=1}^n c_{k_m^<})|G\rangle$, where $k_i^>$ ($k_m^<$) labels an empty (occupied) quasi-particle state in the ground-state, and c_k^\dagger (c_k) creates (destroys) an electron in state $|\psi_k\rangle$. As mentioned above, the excitation changes the electronic charge density within the grain from $\rho_G(\vec{R})$, in the ground-state, to $\rho_{X_n}(\vec{R}) = \rho_G(\vec{R}) - e[\sum_{i=1}^n |\psi_{k_i^>}(\vec{R})|^2 - \sum_{m=1}^n |\psi_{k_m^<}(\vec{R})|^2]$ where \vec{R} indicates an atomic site inside the grain, and $|\psi_k(\vec{R})|^2$ is the wavefunction amplitude of state $|\psi_k\rangle$ at site \vec{R} . Therefore there is an induced (*bare*) charge density in the grain given by: $\delta\rho_{X_n}(\vec{R}) = \rho_{X_n}(\vec{R}) - \rho_G(\vec{R})$ which is *screened* by the electrons present in the metallic grain. This *screening* can be modeled at different levels of complexity.²⁴ Here we implement for simplicity a *static* screening represented by an effective Thomas-Fermi (TF) dielectric constant $\epsilon_q^{TF} = 1 + (q_{TF}/q)^2$ ($q_{TF}^2 = 4(3\pi^5 a_B^3 \mathcal{N})^{-1/3}$ and $q = 2/a_{Al}$ with $a_{Al} = 0.405\text{\AA}$ and $\mathcal{N} = 0.181\text{\AA}^{-3}$ the bulk Al lattice parameter and electronic density, respectively; $a_B = 0.529\text{\AA}$ is the atomic Bohr radius).²⁵ Within this approach the net (screened) induced charge is: $\delta\rho_{X_n}(\vec{R})/\epsilon_q^{TF}$. The choice of the the wave vector magnitude q that enters the TF screening is due to the typical length scale on which the electron wavefunction changes within the grain.⁸

To investigate the effect of the electronic excitations

$\{|X_n\rangle\}$ in the energy spectra of the grain, we extend our tight-binding model by setting the on-site energy of orbital α in atomic site \vec{R}_j to: $\varepsilon_{j\alpha}^{X_n} = \varepsilon_{j\alpha} + \Sigma_{j\alpha}$. Here,

$$\Sigma_{j\alpha} = U_{j\alpha} + \frac{e^2}{\epsilon_q^{TF}} \sum_{i \neq j} \frac{\delta\rho_{X_n}(\vec{R}_i)}{|\vec{R}_i - \vec{R}_j|} \quad (2)$$

is the renormalization energy introduced by the Coulomb interaction due to the electronic excitation. Within the empirical WHM approach discussed above,²⁰ $U_{j\alpha} = (2A_\alpha^j q_j + B_\alpha^j)e\delta\rho_{X_n}(\vec{R}_j)/\epsilon_q^{TF}$, and accounts for the *excess* charge $[-e\delta\rho_{X_n}(\vec{R}_j)/\epsilon_q^{TF}]$ present in atomic site \vec{R}_j due to the redistribution of charge inside the nanograin; q_j is the ground-state charge present in site j . The second term on the right hand side of Eq. (2) is the off-site Hartree contribution.²⁶ It should be noted that in the present model we do not consider any exchange effect—fine structure—that may distinguish between different electron-hole spin configurations. Furthermore, we do not include scattering among different excitations $\{|X_n\rangle\}$. This approximation should be valid for the low-lying electronic excitations.²⁷

IV. CASE STUDY: ALUMINUM NANOGRAINS

We now address the effects of electronic excitations on the energy spectra of metallic nanograins by presenting detailed results for the response of the single-electron energy levels to the creation of the lowest-lying excitations that are accessible at low applied bias voltage in a two-terminal device containing a disc-shaped Al nanograin coated with Al oxide. The grain's volume $\mathcal{V} = 13.4 nm^3$, the drain-source capacitance ratio $C_D/C_S = 1.6$, and the charging energy $U = 4\delta$;²⁸ here $\delta = (4E_F^{Al}/3\mathcal{N})\mathcal{V}^{-1} = 6.3 meV$ is the average energy level spacing—predicted by a particle-in-a-box model of the grain—around the Fermi energy of bulk Al (E_F^{Al}). We consider three representative grains— A , B , and C —that differ in the specific realization of the disorder in their oxide coats.

A. Ground state and excited energy levels

The ground-state ($|G\rangle$) single-electron energy structure of nanograin A is shown in Fig. 2(a); around its Fermi energy (E_F), and for a particular realization of disorder.²⁹ Figure 2(a) also shows the renormalized energy spectra for generation 1 that arise by reaching the threshold voltage $V_{S \rightarrow d}^{th} = V_1^{th}$ to inject an electron into level $|\psi_{E_F+1}\rangle = |1\rangle$; the spectra are labeled by the particular $1eh$ electronic excitation that is involved. For this device at the threshold bias voltage, the resulting singly charged nanoparticle can decay by emitting an

electron from any of seven different single-electron spin-degenerate *orbitals* into the drain contact. As previously discussed, the different excitations renormalize the one-electron energy levels differently; and fluctuations in the magnitude of the energy renormalization, for a given level, are visible. It should be noted that the renormalization of the energy levels is *smaller* than the *average* energy spacing of the ground-state single-electron energy levels:³⁰ $\langle\delta\rangle \simeq 6.9\text{ meV}$. Furthermore, for each *excited* state the average spacing between one-electron energy levels differs from $\langle\delta\rangle$ by less than 2%. Increasing the bias voltage to V_2^{th} , at which it becomes possible for an electron to tunnel into level $|\psi_{E_{F+2}}\rangle = |2\rangle$, leads to *new* 1eh-pair excitations. Figure 2(b) shows in detail—within an energy interval of $3\delta/5$ —the excited single-electron levels around E_{F+1} and E_{F+2} that result from generation 1. For comparison, the box in the lower panel of Fig. 2(b) shows the renormalized energy levels for generation 2; only for E_{F+1} , and at V_1^{th} . Clearly, the fluctuations in the renormalization of the energy levels depend *strongly* on the details of the excitation(s) that are involved.

As mentioned above, disorder imparts a stochastic nature to the confined electronic wavefunctions, thus dramatically affecting the renormalization fluctuations. The latter are visible in Figure 3, where the ground-state and excited electronic energy levels for different disorder realizations are shown: While for grain *A* the spectra show one of the renormalized levels of E_{F+1} and E_{F+2} visibly separated from the others, for all these 1eh-pair excitations, this is not the case for *B* and *C*; see Fig. 3. In particular, for grain *C*, the renormalized energy levels corresponding to E_{F+2} , at V_2^{th} , superpose with the renormalized levels for E_{F+3} . It should be noted that the number of excitations is similar for the different nanograins. This results from the combined effect of (i) adopting the same drain-source capacitance ratio ($C_D/C_S = 1.6$) and charging energy ($U = 4\delta$) for all the grains, and (ii) having the volume (\mathcal{V}) fixed while changing the disorder from grain to grain. The latter gives nearly the same *average* number of single-electron energy levels in an energy interval of *several* δ for each grain.⁷ In particular, the number of available orbitals for generating excitations, at V_1^{th} , is roughly: $\text{int}\{[U + E_{F+1} - E_F][1 + (C_D/C_S)^{-1}]/\delta\} = \text{int}\{6.5 + 1.625(E_{F+1} - E_F)/\delta\}$, where $\text{int}(x)$ is the integer part of x .

In conclusion, the response of the electronic structure to the excitations exhibits strong dependence on the energy levels involved in the excitation, and disorder realization.

B. Differential conductance

Having calculated the renormalized energy levels let us turn now to the implications for the differential conductance. We concentrate here on finding the energies—or, equivalently, bias voltage—at which tunneling resonances should be present rather than performing an actual cal-

culcation of the dI/dV spectrum. The latter is beyond the scope of this work as it would require to solve a complicated master equation describing the kinetics of the tunneling transitions far from equilibrium.

In general, resonances in dI/dV arise when new channels for tunneling open as the bias voltage is swept. In the Coulomb blockade regime, three kinds of tunneling resonances are expected in the spectra of metal nanograins: Direct, charge-fluctuation,⁸ and non-equilibrium.⁵ The first two are present regardless of the ratio between the electronic relaxation and bottleneck tunneling rate, therefore they are regarded as *equilibrium* resonances. Direct resonances generally correspond to tunneling transitions directly into (out of) an electronic energy level in the ground state of the nanograin. The charge-fluctuation resonances that are present at low bias voltage arise from having a finite probability for the nanograin to be (on average) negatively charged—excess of one electron.⁸ These resonances are also non-trivially affected by non-equilibrium effects (see below), however, they were *not included* in the original AWARTi model. Here, we generically label them Q^+ .

Figure 4 summarizes the bias voltages (V), presented in units of energy after converting to eV , at which tunneling resonances should be present in the dI/dV spectra of grains *A*, *B*, and *C*; at low bias voltage. Resonances appear in groups: three in *A*, and two in *B* and *C*; only $G\neq 0$ (ground-state) and $G\neq 1$ are shown. In these grains the Fermi level is doubly occupied, as mentioned in Sec. II; furthermore, the adopted capacitance ratio C_D/C_S is such that in these devices the onset of tunneling takes place when an electron is injected from the source electrode into the grain. Hence, the first resonance in dI/dV appears when the bias voltage reaches V_1^{th} . Upon increasing V , an additional *non-equilibrium* tunneling resonance appears in the spectrum each time a renormalized energy value of E_{F+1} is reached. Further increase in the bias voltage results in new equilibrium and non-equilibrium resonances that arise from tunneling into E_{F+2} (at V_2^{th}) and its renormalized energy levels, respectively. Non-equilibrium resonances appear as satellites of the main, equilibrium, resonances due to tunneling into E_{F+1} and E_{F+2} . This leads to group 1 and 3 in *A*; 1 and, partially, group 2 in *B*; and group 1 and 2 in *C*. It should be noted that the satellites involving level E_{F+2} , however, do not systematically appear above the equilibrium resonance. The latter would make the experimental identification of the equilibrium resonance difficult. Moreover, the number of such satellite resonances is *bigger* than in the neighborhood of V_1^{th} as the accessible 1eh-pair excitations at V_2^{th} involve both levels E_{F+1} and E_{F+2} . Finally, at bias voltages greater than V_1^{th} the finite probability to have the nanoparticle *negatively* charged leads to charge-fluctuation resonances⁸ (equilibrium and non-equilibrium satellites) that are responsible for group 2 (Q^+) in *A*, and part of group 2 in *B*. However, no Q^+ resonances are present in grain *C* as a consequence of its electronic structure below the Fermi

energy.³¹ It is also noticeable that in grain C the clusters of resonances are less dense than in A and B although the number of 1eh-pair excitations is nearly the same in all grains, as discussed above. This shows the high sensitivity of the tunneling spectrum to the response of the electronic energy level structure to eh excitations, and to the disorder present in the grain.

If we were to include in the above discussion of the dI/dV spectrum the renormalized energy levels corresponding to $G\#2$ [see Fig. 2(b)] this would dramatically increase the number of non-equilibrium resonances. In fact, if the kinetics of the tunneling transitions is such as to admit a significant population of excited states then it should be possible to achieve much higher spectral densities of tunneling resonances than observed to date, simply by increasing the thickness of the tunnel barriers and hence the tunneling time relative to the relaxation time of the eh pair excitations. This kinetics is determined by microscopic parameters of the grain, and the nature of the electron-phonon scattering within it; which strongly depend on the volume of the grain (see Ref. 32) and disorder. Hence, there is no *a priori* (during the growth) control on the expected number of non-equilibrium resonances during charge transport in a device. Nonetheless, tunneling experiments in gated devices (as those reported in Ref. 33), where the *charging energy* of the device may be changed with the applied gate voltage, should at least be able to address the increase of the number of non-equilibrium resonances as a function of the available orbitals (N ; see Sec. II) to generate the electronic excitations. Such observations may be contrasted with the predicted number of excitations in generation n as a function of N ; see Sec. II. However, the details of the renormalization of the probed energy level may hinder such a comparison. [see Fig. 3 and 4, grain C , where the number of non-equilibrium resonances in the first cluster is smaller (nearly 1/2) than the number of accessible excitations, as a result of having some renormalized levels (spectrally) below E_{F+1} . The latter implies that these excitations contribute to determine the tunneling current at V_1^{th} , rather than adding satellite resonances into the dI/dV spectrum.]

To summarize, the high sensitivity of the ground-state and excited electronic energy spectrum to disorder is non-trivially inherited by the differential conductance spectrum: (i) The number of neutral tunneling resonances (equilibrium and non-equilibrium) strongly depend on the response of the electronic energy levels to the excitations. (ii) Charge-fluctuation resonances appear in clusters that, depending on disorder, can *overlap* with the neutral non-equilibrium resonances, as shown in Fig. 4 (grain B). This would increase the complexity of the tunneling spectrum and make the interpretation of experiments difficult.

V. SUMMARY

In summary, we have presented a systematic study of the tunneling-induced electronic excitations in non-

magnetic metallic nanograins: (i) We have discussed the mechanism that creates electronic excitations and classified them according to the resulting number of electron-hole pairs, which enabled us to introduce the concept of generations of excitations: A subspace of excitations with a specific number of electron-hole pairs. The generations form a hierarchy, and the number of elements in a generation is determined by the applied bias voltage and characteristics of the device. (ii) We have proposed a general microscopic mean-field model that can be used to calculate the quasi-particle energy levels in the presence of a tunneling-induced excitation. Based on this model, we have presented detailed results for the response of the electronic structure of ultra-small aluminum grains coated with Al oxide to these excitations. However, the model should be applicable to most of the non-magnetic metallic nanograins currently probed in tunneling spectroscopy experiments. Our results show that disorder present at the surfaces of the nanograins imparts a fluctuating character to the renormalization of the single-electron energy levels due to the excitations, and that this renormalization is smaller than the typical energy spacing between single-particle levels. Furthermore, the tunneling spectra of the nanograins consist of equilibrium and non-equilibrium resonances, which appear in clusters whose structure is dramatically affected by the high sensitivity of the ground-state and excited electronic energy structure to disorder.

We have also shown that if the nonequilibrium resonances discussed here and in previous work⁵ are present in the tunneling spectra of metal nanoparticles at all, then their density in the spectra should vary *greatly* from sample to sample. This is because (a) the density of nonequilibrium resonances increases rapidly with the number of *generations* of excited states that are populated in the nanograin and (b) this number of populated generations is in turn very sample dependent.

Finally, we have suggested that tunneling spectroscopy experiments in gated ultrasmall nanograins may be useful to probe the variation in the number of non-equilibrium resonances as a function of the number of available orbitals for tunneling.

Acknowledgments

We are grateful to John W. Wilkins for his helpful comments. Funding from U. S. DOE grant DE-FG02-99ER45795 made it possible to complete this research at The Ohio State University. The work at Simon Fraser University—where this research started—was funded by the Natural Science and Engineering Research Council (NSERC), and the Canadian Institute for Advanced Research (CIAR).

- ¹ D. C. Ralph, C. T. Black, and M. Tinkham, Phys. Rev. Lett. **74**, 3241 (1995); Phys. Rev. Lett. **78**, 4087 (1997)
- ² D. Davidović and M. Tinkham, Phys. Rev. B **61**, R16359 (2000)
- ³ J. R. Petta and D. C. Ralph, Phys. Rev. Lett. **87**, 266801 (2001); *ibid*, Phys. Rev. Lett. **89**, 156802 (2002)
- ⁴ S. Guéron, M. M. Deshmukh, E. B. Myers, and D. C. Ralph Phys. Rev. Lett. **83**, 4148 (1999); M. M. Deshmukh, S. Kleff, S. Guéron, E. Bonet, A. N. Pasupathy, J. von Delft, and D. C. Ralph Phys. Rev. Lett. **87**, 226801 (2001); M. M. Deshmukh and D. C. Ralph, Phys. Rev. Lett. **89**, 266803 (2002)
- ⁵ O. Agam, N. S. Wingreen, B. L. Altshuler, D. C. Ralph, and M. Tinkham, Phys. Rev. Lett. **78**, 1956 (1997)
- ⁶ A. H. MacDonald, C. M. Canali, Solid State Comm. **119**, 253 (2001); C. M. Canali and A. H. MacDonald, Phys. Rev. Lett. **85**, 5623 (2000); S. Kleff, J. von Delft, M. M. Deshmukh, and D. C. Ralph, Phys. Rev. B **64**, 220401(R) (2001); I. L. Aleiner, P. W. Brouwer and L. I. Glazman, Phys. Rep. **358**, 309 (2002); E. Bonet, M. M. Deshmukh, and D. C. Ralph, Phys. Rev. B **65**, 045317 (2002); J. von Delft and D. C. Ralph, Phys. Rep. **345**, 61 (2001)
- ⁷ G. A. Narvaez and G. Kirczenow, Phys. Rev. B **65**, 121403(R) (2002)
- ⁸ G. A. Narvaez and G. Kirczenow, Phys. Rev. B **66**, 081404(R) (2002)
- ⁹ G. A. Narvaez and G. Kirczenow, Phys. Rev. B **67**, 195409 (2003)
- ¹⁰ T. A. Brody, J. Flores, J. B. French, P. A. Mello, A. Pandey, S. S. M. Wong, Rev. Mod. Phys. **53**, 385 (1981); K. B. Efetov, Adv. Phys. **32**, 53 (1983); W. P. Halperin, Rev. Mod. Phys. **58**, 533 (1986); A. D. Mirlin, Phys. Rep. **326**, 260 (2000); Y. Alhassid, Rev. Mod. Phys. **72**, 895 (2000);
- ¹¹ K. K. Likharev, IBM J. Res. Dev. **32**, 144 (1988); Proc. IEEE **87**, 606 (1999); D. V. Averin and K. K. Likharev, in *Mesoscopic Phenomena in Solids*, Eds. B. L. Altshuler, P. A. Lee, and R. A. Webb (Elsevier, Amsterdam, 1991); G.-L. Ingold and Yu. Nazarov, in *Single Charge Tunneling*, Eds. H. Grabert and M. H. Devoret, (Plenum, NY, 1991);
- ¹² This simplification *does not* change the genesis process of the electronic excitations.
- ¹³ D. Ullmo and H. U. Baranger, Phys. Rev. B **64**, 245324 (2001)
- ¹⁴ G. D. Mahan, *Many-Particle Physics* (Plenum, New York, 1990)
- ¹⁵ J. C. Slater and G. F. Koster, Phys. Rev. **94**, 1498 (1954)
- ¹⁶ We adopt an Slater-Koster model in which the atomic orbitals on different sites are orthonormal, and consider hopping up to second nearest neighbors. The Hamiltonian is diagonalized by using a Lanczos algorithm [for an implementation see: J. K. Cullum and R. A. Willoughby, *Lanczos Algorithms for Large Symmetric Eigenvalue Computations*, Birkhäuser (Boston, Basel, Stuttgart, 1985)]
- ¹⁷ State-of-the-art molecular dynamics suggest that there is an amorphization on the metal-oxide interface rather than crystalline surface reconstructions—see Ref. 21.
- ¹⁸ In this model, the geometry can be arbitrary. However, discs and hemispheres are the most widely assumed geometries in the literature. On the other hand, our choice of an fcc lattice host is consistent with the bulk lattices of most of the metals studied experimentally at present.
- ¹⁹ D. A. Papaconstantopoulos, *Handbook of the Band Structure of Elemental Solids* (Plenum Press, 1986)
- ²⁰ S. P. McGlynn, L. G. Vanquickenborne, M. Kinoshita, and D. G. Carrol, *Introduction to Applied Quantum Chemistry* (Holt, Rinehart and Winston, New York, 1972)
- ²¹ T. Campbell, R. K. Kalia, A. Nakano, P. Vashishta, S. Ogata, and S. Rodgers, Phys. Rev. Lett. **82**, 4866 (1999)
- ²² W. A. Harrison, *Electronic Structure and the Properties of Solids-The Physics of the Chemical Bond*, W. H. Freeman and Company (San Francisco, 1980)
- ²³ S. Ansell, S. Krishnan, J. K. Richard Weber, J. J. Felten, P. C. Nordine, M. A. Beno, D. L. Price and M.-L. Saboungi, Phys. Rev. Lett. **78**, 464 (1997)
- ²⁴ Ya. M. Blanter, A. D. Mirlin, and B. A. Muzykantskii, Phys. Rev. Lett. **78**, 2449 (1997)
- ²⁵ N. W. Ashcroft and D. N. Mermin, *Solid State Physics* (Saunders, Philadelphia, 1976)
- ²⁶ While more sophisticated accounts for the *screening* ($\Sigma_{j\alpha}$) may be implemented the results derived from this simple model should be qualitatively correct.
- ²⁷ B. L. Alshuler, Y. Gefen, A. Kamenev, and L. S. Levitov, Phys. Rev. Lett. **78**, 2803 (1997)
- ²⁸ These numbers correspond to typical parameters for the smallest available nanoparticles (see Refs. 1,2,3,4).
- ²⁹ E_F changes a few tens of *meV* when switching from one disorder realisation to another.
- ³⁰ This spacing is calculated by considering 200 energy levels in the ground-state, symmetrically located around E_F .
- ³¹ In general, Q^+ originate from opening conduction channels that involve energy levels in the neighborhood of $\mu_D(V) - U$ below E_F . See Ref. 8 for details.
- ³² A. Arbouet *et al.*, Phys. Rev. Lett. **90**, 177401 (2003)
- ³³ M. M. Deshmukh, E. Bonet, A. N. Pasupathy, and D. C. Ralph, Phys. Rev. B **65**, 073301 (2002). In the latter paper, the probed grains have typical diameters of about $10nm$ which make difficult to address the non-equilibrium satellite resonances individually.

FIG. 1: (a) Mechanism for creating electronic excitations, exemplified with the creation of a 1eh-pair excitation: from the source (S) electrode, an electron tunnels into energy level $|\psi_{F+1}\rangle = |1\rangle$ of an originally neutral grain containing n_0 conduction electrons in its ground state $|G\rangle$, with a charging energy U as represented in the plot; the grain gets negatively charged ($n_0 \rightarrow n_0 + 1$), and the single-electron energy levels are renormalized by an amount U ; subsequently, an electron tunnels out—from, in this example, level $|\psi_{F-1}\rangle = |\bar{1}\rangle$ —to the drain (D) contact which leaves the nanoparticle in an electronic excited state: $|1; \bar{1}\rangle = c_1^\dagger c_{\bar{1}} |G\rangle$. In the latter notation, c_1^\dagger ($c_{\bar{1}}$) creates (destroys) an electron in state $|1\rangle$ ($|\bar{1}\rangle$). (b) $G\#1$ and $G\#2$ are representative elements of generation 1, containing 1eh-pair excitations, and generation 2, corresponding to 2eh-pairs; details in text. $|11; \bar{1}\bar{3}\rangle = c_1^\dagger c_1^\dagger c_{\bar{1}} c_{\bar{3}} |G\rangle$ is pictorially present in this example. (c) Schematic representation of the renormalization of the ground-state single-electron energy levels after generating excitation $|1; \bar{1}\rangle$ —see text. The renormalized energy levels are shown as dotted dashes.

FIG. 2: (a) Energy levels for grain A (volume $\mathcal{V} = 13.4 \text{ nm}^3$) around the Fermi energy (E_F) of the ground-state grain in units of $\delta = 6.3 \text{ meV}$ —the average electron-in-a-box energy level spacing—for the ground-state ($|G\rangle$, bold dashes) and different one electron-hole pair excitations ($|X_1\rangle = c_k^\dagger c_{k'} |G\rangle = |k; \bar{k}'\rangle$; k and k' indicate the (excited) electron and (excited) hole one-electron levels, respectively. Thin dashes.) that may be created after the applied bias voltage reaches the threshold for tunneling an electron into level $|1\rangle$ in the neutral grain from S : V_1^{th} . (b) Details of the renormalization of levels $|\psi_{F+1}\rangle$ and $|\psi_{F+2}\rangle$ arising from the presence of 1eh-pair excitations at V_1^{th} and V_2^{th} —bias voltage to tunnel an electron into $|\psi_{F+2}\rangle$ from S . The box marks the renormalized energy of single-electron level $|1\rangle$ that results from 2eh-pairs excitations. Full scale corresponds to energy interval of $3\delta/5$.

FIG. 3: Ground state $|G\rangle$ (bold dashes) and excited single-electron energy levels (thin dashes) for different realizations of disorder—grains A , B , and C . Excited states belong to $G\#1$ (1eh-pair excitations), at bias voltages V_1^{th} and V_2^{th} (see text and caption of Fig. 2). The renormalization of the energy levels shows a strong sample (disorder realization) variation. Notice the different energy scales in the plots. E_F is the Fermi energy of each grain, and δ is the same as defined in Fig. 2.

FIG. 4: Applied bias voltages (converted to energy: eV) derived from the calculated ground-state and excited energy spectra at which tunneling resonances would appear in the dI/dV spectrum of the studied devices (see text). Only generations 0 ($G\#0$) and 1 ($G\#1$) are considered when finding the energies for direct and charge-fluctuation (equilibrium and non-equilibrium) resonances. Thin and bold (blue in on-line version) bars distinguish between energies associated with direct and charge-fluctuation resonances, respectively. Different heights mark equilibrium and non-equilibrium resonance energies: $3/2$ and $3/4$ for the former, while 1 and $1/2$ label the latter. In the top panel—grain A —the symbol Q^+ indicates a cluster of charge-fluctuation resonances (see text, and Ref. 8). The * indicates nearly-degenerate values of eV. The ordinate scale is the same in all panels, however, notice the different range of bias voltages in each plot. U and δ have the same meaning as in the previous figures.

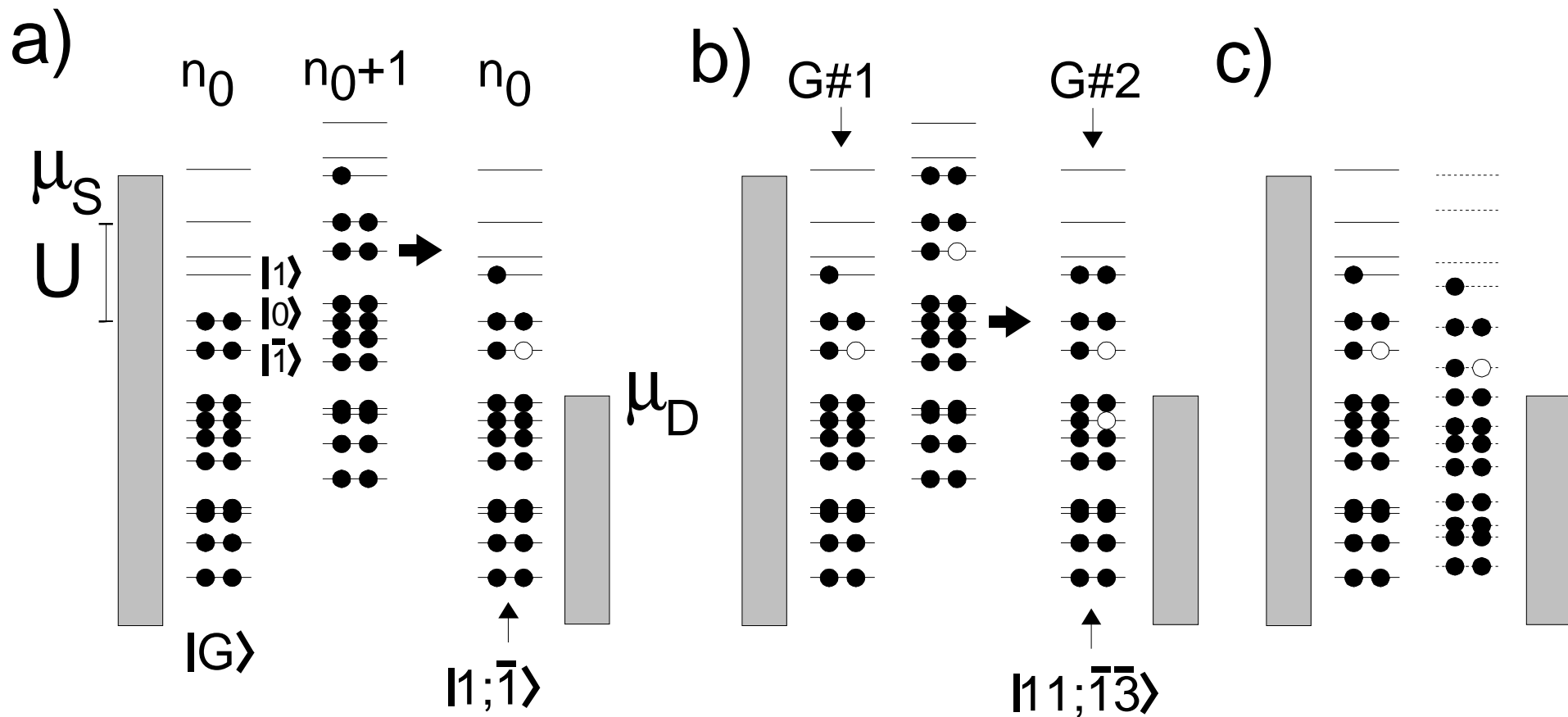


Figure 1, Narvaez and Kirczenow

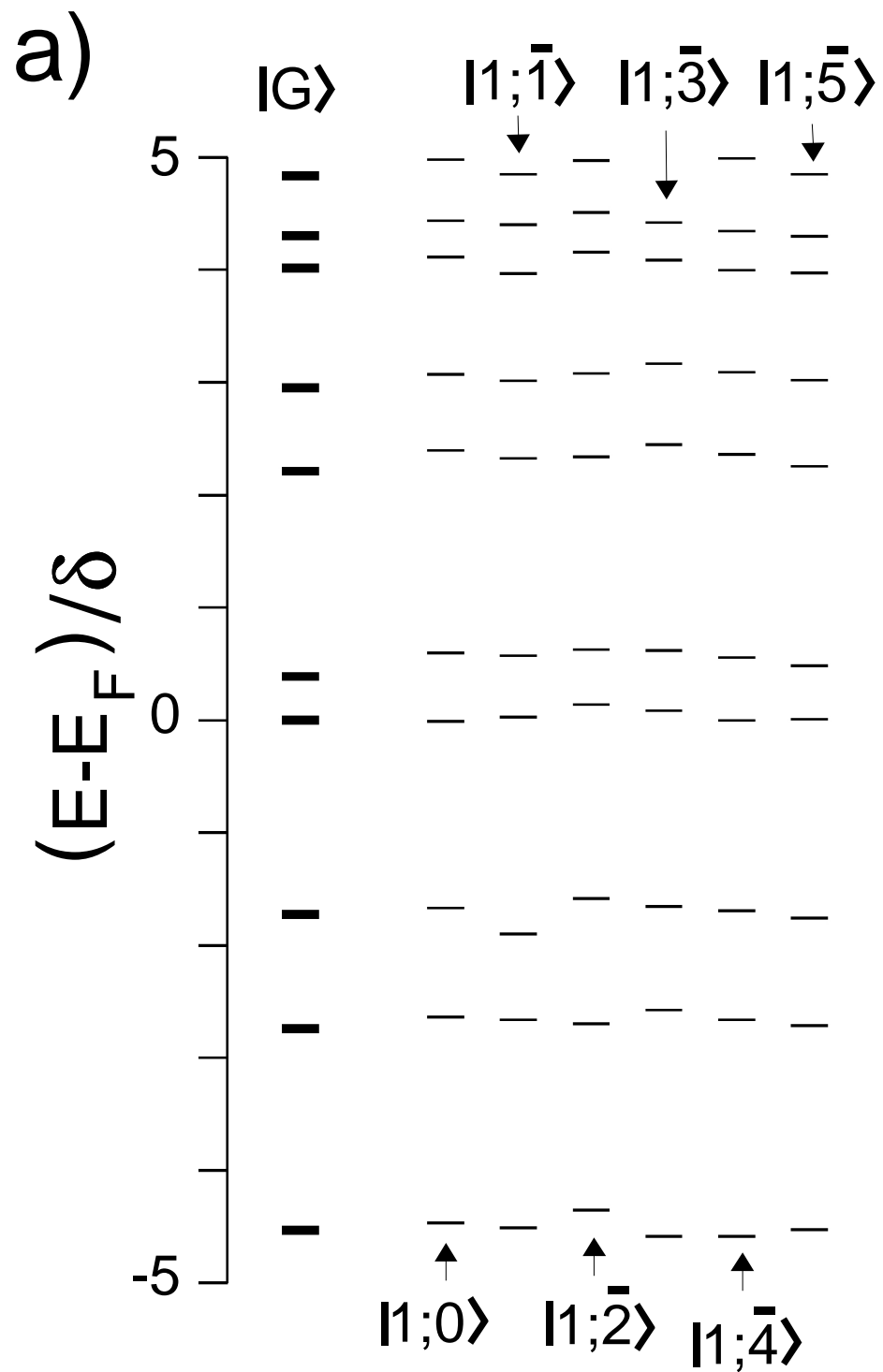


Figure 2, Narvaez and Kirczenow

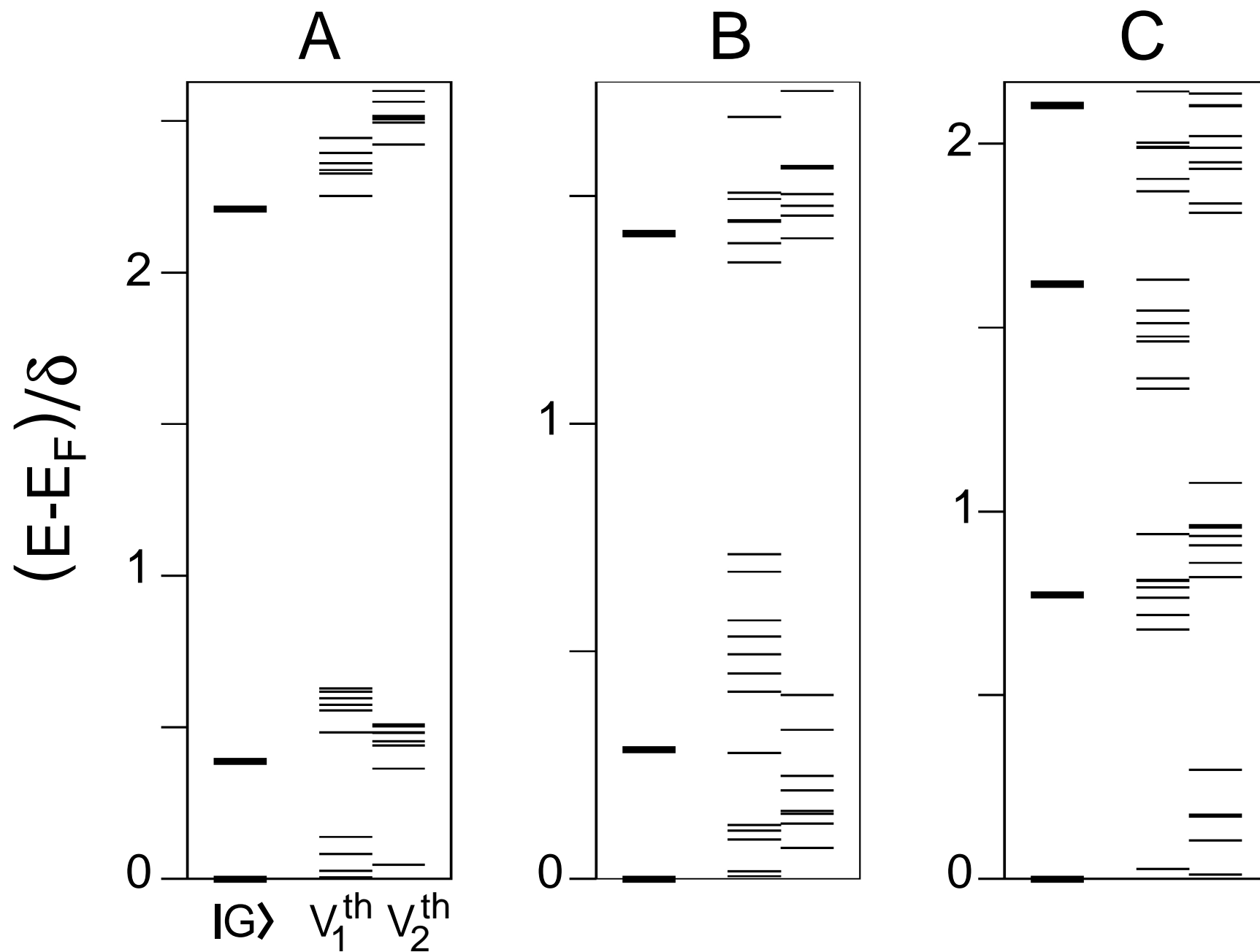


Figure 3, Narvaez and Kirczenow

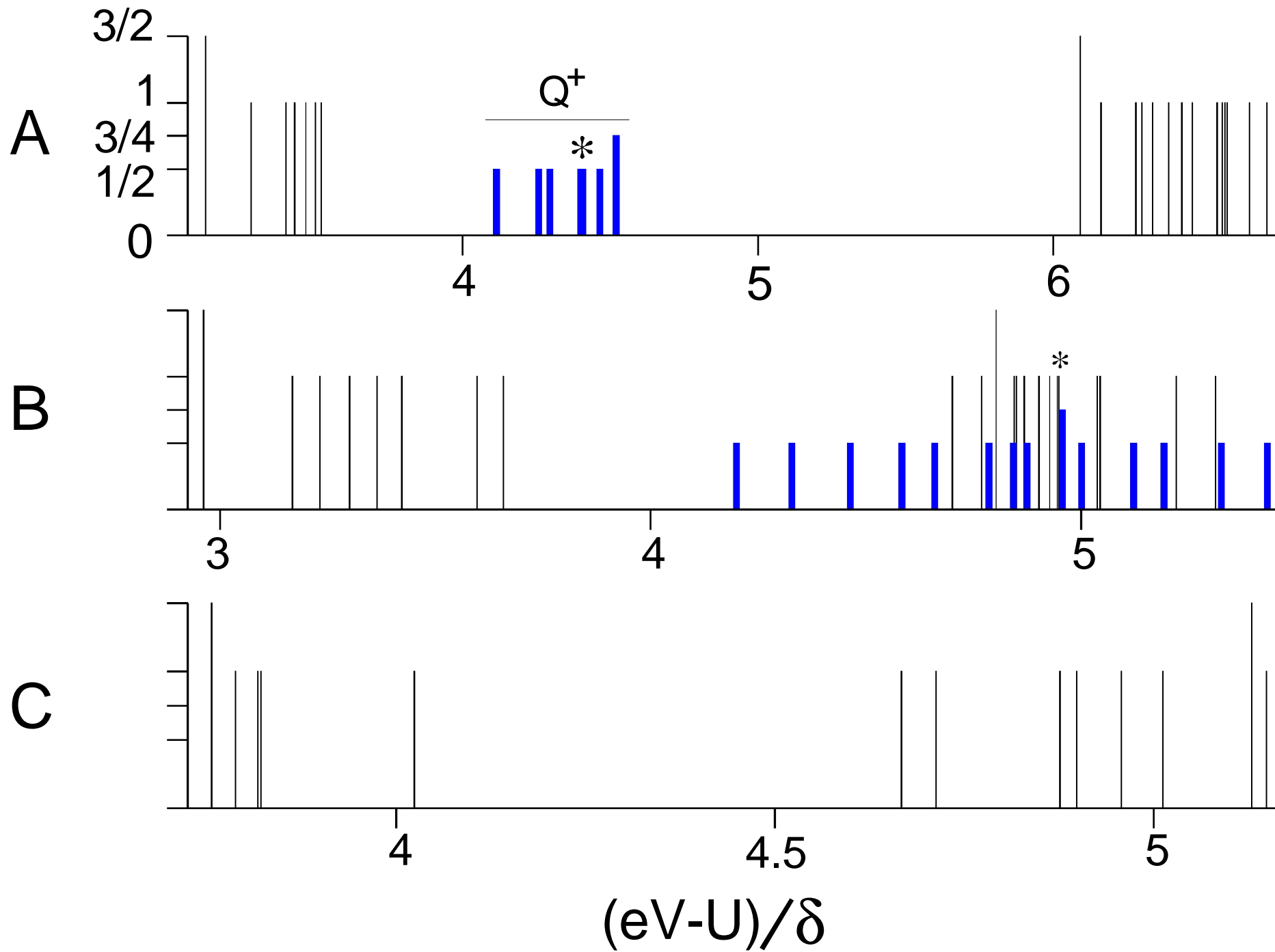


Figure 4, Narvaez and Kirczenow